7th IAA Planetary Defense Conference - PDC 2021
26-30 April 2021, Vienna, Austria

IAA-PDC-21-01-88

CISLUNAR DEPARTURE EXPLOITATION FOR PLANETARY DEFENSE MISSIONS DESIGN

Pasquale Andrea[1], Lavagna Michèle[2], and Florian Renk[3]

[1] *Politecnico di Milano, Via La Masa, 34, 20156 Milan – Italy, andrea.pasquale@polimi.it*
[2] *Politecnico di Milano, Via La Masa, 34, 20156 Milan – Italy, michelle.lavagna@polimi.it*
[3] *ESA/ESOC Mission Analysis Section, Robert-Bosch-Str 5, 64293 Darmstadt – Germany, florian.renk@esa.int*

Abstract

Since some years, issues and challenges related to planetary defense raise awareness on the community. This paper discusses a possible strategy - and its derived requirements to be satisfied - to exploit the Cislunar environment as departing outpost for planetary defense missions.

Three relevant scenarios are investigated, to prove the flexibility of a Cislunar departure and to point out the different geometrical and dynamical requirements that each category imposes: a kinetic impact mission case, driven by the departure energy minimisation and the impact geometry optimization, with the subsequent impact effects evaluation at the Earth MOID; a fly-by mission case, focused on minimizing the transfer energy and maximizing the flyby time, with the aim at hopping multiple bodies and favouring an high scientific return from each flyby; a rendez-vous mission case, aimed at minimizing the total transfer energy.

To make the analysis statistically relevant a synthetic population has been generated and appended to the real set, accounting for Near-Earth Objects and Potentially Hazardous Objects not discovered yet. Then, a Lambert – based optimisation is performed on the augmented population for each of the aforementioned cases: the paper shows the parameters cross correlations tables and the cumulative distributions identified built to quickly detect the set of reachable objects, according to the parameters values selection.

The strategy to drive the design of the subset of Cislunar direct departing trajectories that best match the departure conditions at the Earth-Moon SOI, given by the previously computed Lambert arcs, is also presented. Some relevant cases among the three scenarios are also discussed in details.

Keywords: astrodynamics, trajectory design, asteroid deflection mission, planetary defense, Near-Earth Objects reachability maps

1. Introduction

In the last years the attention of the scientific community to the objects on Earth-crossing orbit has increased, and, more generally, to those having perihelion distances $q \leq 1.3AU$ and aphelion distances $Q \geq 0.983AU$, which compose the usually called Near Earth Objects (NEO) population. As a consequence, there have been a number of surveys with the goal to search and characterize >90% of the NEO population with a diameter greater than 1 km, with a recent studies aimed to increase this level to >90% of the bodies down to 100 m in diameter [1, 2]. Moreover, many NEOs are classified as Potentially Hazardous Objects (PHO), and could pose a threat to our planet. In this context, according to the Global Exploration Roadmap, the characterization of potential near-Earth asteroid collision threats, and test techniques to mitigate the risk of asteroid collisions with Earth are fundamental objectives for this decade. For this reason there are a number of missions that had target objects in this region [3, 4, 5, 6] as well as a number of proposed missions for the near future [7].

In this context, according, again, to the Global Exploration Roadmap, ISECG agencies have become increasingly interested and committed in implementing long-term sustainable missions based on international cooperation and commercial participation in the cislunar space: the lunar Gateway (LOP-G) program is a clear example. The LOP-G will serve, in fact, not only as a test-bed for the future manned missions to Mars but also to enable sustainable living and working about and on the Moon, stimulating the industrial competitiveness for space exploration. For these reasons, many studies have been devoted to the characterisation of Cislunar multi-body orbital families, dedicated to Earth visibility and accessibility [8, 9, 10] but also to interplanetary transfer design departing from the Cislunar space [11, 12]. Recently, studies on the Near-Earth Objects reachability for limited-resources platforms (mostly Cubesats) exploiting solar electric propulsion have been published [13, 14].

This paper presents a preliminary analysis of the reachability of NEAs, considering three possible scenarios: a rendezvous, a flyby and a kinetic impact geometry optimization. The study is performed over a lunch window spanning from 2025 to 2040 and include all the known NEA ($\sim$ 25000) as well as a synthetic population composed by 10000 synthetic bodies, to account for bodies that have not been discovered yet. A statistical analysis of the resulting escape conditions is performed and compared to Earth-Moon Libration Points escape conditions. The fraction of reachable object from the Cislunar environment is then recovered.

The article is structured as follows. In Section 2, a brief description of the NEA population and the synthetic family generation is presented. The NEA's Mission specific models are then presented in Section 3. Section 4 presents the simulation environment considered for the analysis while Section 5 the analysis of the results.

2. The NEA Population and the Synthetic Family

With the observation data available from NASA JPL Small-Body Database and Mi-nor Planet Center Database, in this section the Near-Earth Asteroids (NEA) and Potentially Hazardous Asteroids (PHA) populations are extracted and briefly analyzed. The resulting group of 25493 NEA and 2155 PHA (approx 10% of NEA are PHA) is identified merging the two databases and is represented in Fig. 1 by means of its most relevant parameters. Note that here the orbital parameters exhibit a clear correlation

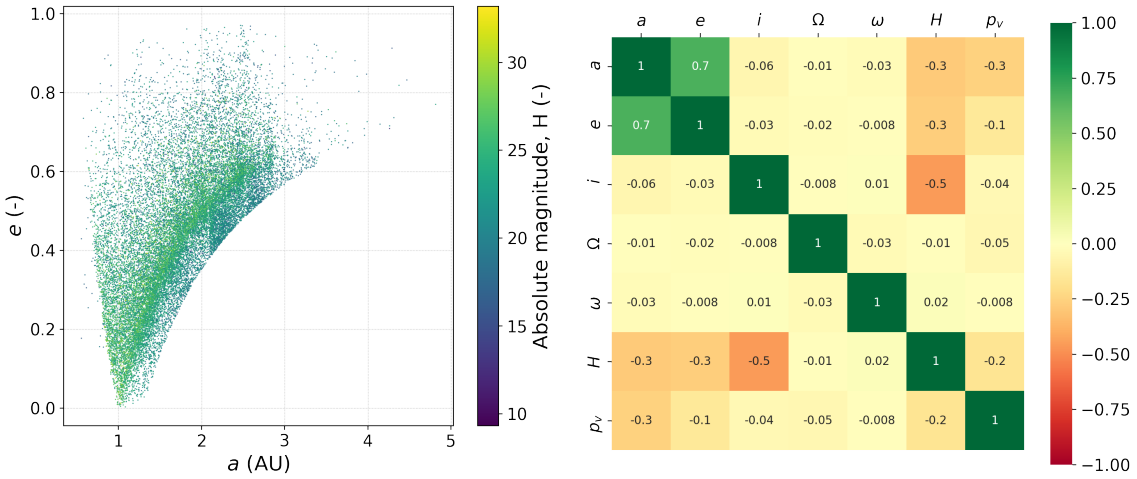

(a) a-e correlation. **(b) Pearson correlation matrix.**

Figure 1. NEA family and its relevant parameters cross-correlation. Here $(a, e, i, \Omega, \omega)$ are the osculating orbit parameters, H the absolute magnitude and p_v the geometric albedo.

are a and e whereas the others may be considered as statistically uncorrelated. Moreover can be shown that Ω and ω are practically random quantities while the inclination has a distribution such that most of NEA ($\sim$ 90%) are within an inclination of 25° to the ecliptic.

2.1. The Synthetic Family

In line with [15, 16], for the generation of a synthetic population of NEA it is assumed that:

- The correlation between the albedo (p_V) and absolute magnitude (H) is not statistically significant;
- No statistically significant correlation between albedo and orbital eccentricity or inclination.
- The conversion between absolute magnitude and diameter is given by:

$$H = 15.618 - 5\log_{10} D - 2.5\log_{10} p_V \tag{1}$$

This implies that all quantities a and e can be considered uncorrelated. However, within this study, it is assumed that *all* quantities are statistically uncorrelated, allowing to generate the synthetic group in a simple way, i.e. directly from the probability density function (pdf) associated to each of the parameters. The estimation of the pdf is performed in a simple way with a Kernel Density Estimation (KDE) from the data available [17]. However, for the generation of adequate synthetic objects, some constrains must be imposed. Then, two groups of constrains are imposed:

1. *Physical constraints*: $e > 0$, $a > 0$ if $e < 1$, $q < a$, $Q > a$ etc.

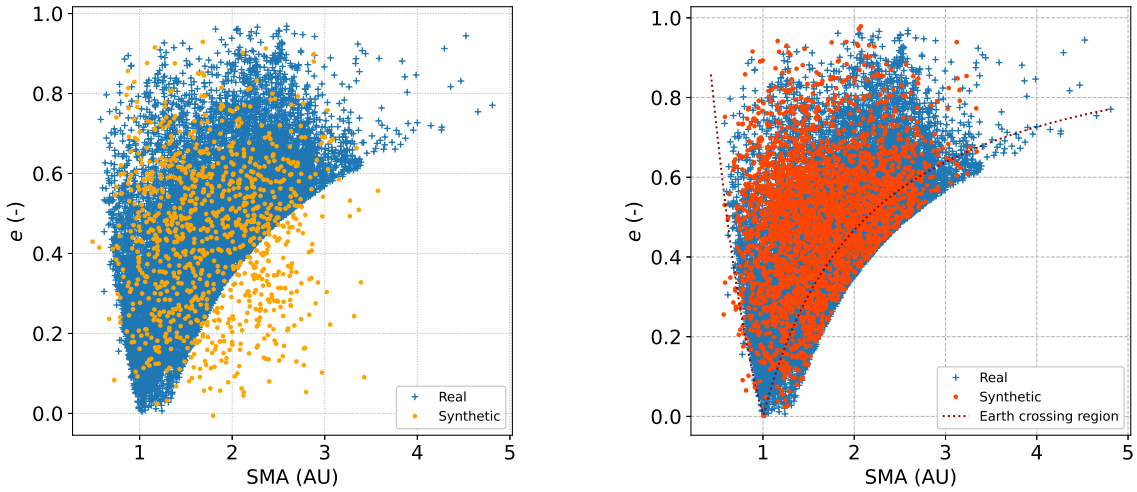

(a) "NEO constraint" inactive. **(b) "NEO constraint" *active*.**

Figure 2. Synthetic family constraint effect example.

2. *Category constraints*: for example, if the objects into analysis are *Apollos*, the $a\,pdf$ is mixed with the constraint $a > 1AU$ and instead of the $e\,pdf$ the distribution of the pericenter radius q is computed and mixed with the constraint $q < 1.017\,AU$. The $e\,pdf$ is then recovered from the (a, q) ones.

Where here q and Q are the pericenter and apocenter radii respectively. An example of the aforementioned constraints is provided in Fig. 2.

In this study, the population formed by real and synthetic objects will be called *augmented population*.

3. NEO Missions Cases Definition and Modelling

In this section the three mission cases and their relevant quantities for a preliminary mission design are described.

3.1. Rendezvous

The first mission scenario considered in this paper is a rendezvous mission (RV). In this paper this case corresponds simply to the total transfer energy optimization, i.e. the total ΔV minimization.

3.2. Flyby

The second mission scenario considered a Flyby (FB) mission. In this case a two layer optimization is adopted.

1. In the first layer, the departure energy in optimized or, equivalently, V_∞ is minimized.

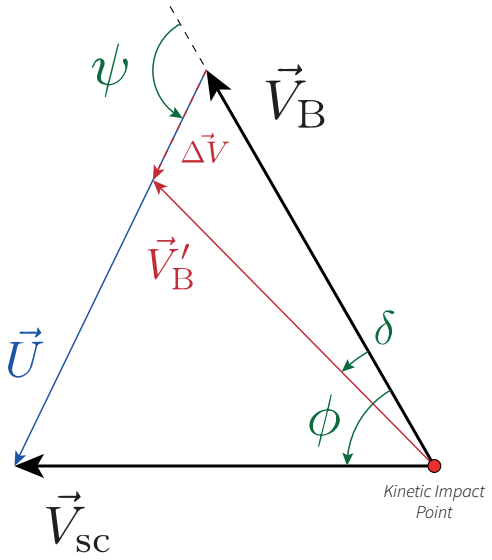

Figure 3. Planar kinetic impact geometry.

2. In the second layer, instead, taking as initial guess the result of the previous layer, a constrained optimization of the arrival relative velocity $\mathbf{U}$ is performed with the aim to reduce it at the most (to increase the FB time and thus increase the scientific return).

3.3. Kinetic Impact

The third mission scenario is considered to be a Kinetic Impact (KI) mission. In this paper the objective of this case is to maximize the deflection achieved by the KI.

According to several authors [18, 19, 20], a KI can be considered inelastic, so that the conservation of total momentum must be satisfied across the impact. To take into account the cratering and the complex ejecta dynamic, a *momentum transfer efficiency* factor β is usually introduced. According to [18] the momentum carried off by crater ejecta can lead to $\beta > 3$. With that in mind, the total momentum conservation law reads:

$$\beta(m\mathbf{V}_{\mathrm{sc}} + M\mathbf{V}_B) = (m + M)(\mathbf{V}_B + \Delta\mathbf{V}) \tag{2}$$

This equation can be rewritten in a more practical form as:

$$\Delta\mathbf{V} = \kappa\mathbf{U} \tag{3}$$

where κ will be called *momentum factor* and correspond, given β, the mass of the Body M and the mass of the Spacecraft at the impact, m, to:

$$\kappa = \beta\frac{m}{m + M} \tag{4}$$

while $\mathbf{U}$ is the *Spacecraft impact relative velocity*, given by:

$$\mathbf{U} = \mathbf{V}_{\mathrm{sc}} - \mathbf{V}_B \tag{5}$$

With reference to Fig. 3, in this paper we assume to model the effects of the impact with a qualitative approach from the energetic point of view. Defining:

- *Impact angle*, ϕ: angle between the S/C and the Body velocity at Impact Point.
- *Deflection angle*, δ: angle between the Body velocity before and after the Impact.
- *Acceleration angle*, ψ: angle between the Body velocity and the ΔV.

And assuming that $m \ll M$ so that $m+M \approx M$, the *vis-viva* equation before and after the impact can be written as:

$$\mathcal{E}_{\text{pre}} = \frac{1}{2}V_B^2 - \frac{\mu}{r} \tag{6}$$

$$\mathcal{E}_{\text{post}} = \frac{1}{2}||\mathbf{V}_B + \delta\mathbf{V}||^2 - \frac{\mu}{r} \tag{7}$$

Where all quantities are taken at the KI Point. If the objective of the impact is to change the orbital energy, then the delta-energy must be studied. In this case, defining $\Delta\mathcal{E} = \mathcal{E}_{\text{post}} - \mathcal{E}_{\text{pre}}$, then:

$$\Delta\mathcal{E} = \frac{1}{2}\delta V^2 + \mathbf{V}_{\text{B}} \cdot \Delta\mathbf{V} \tag{8}$$

But since $\Delta\mathbf{V} = \kappa\mathbf{U}$, then:

$$\Delta\mathcal{E} = \frac{1}{2}\kappa^2 U^2 + \kappa\mathbf{V}_{\text{B}} \cdot \mathbf{U} \tag{9}$$

Note that since $\kappa \ll 1$, the first term can be neglected so that the effect of the impact reads, after some manipulation:

$$\Delta\mathcal{E} \approx \kappa V_B^2 \left(\frac{V_{\text{sc}}}{V_B}\cos\phi - 1\right) \tag{10}$$

Then, since the kinetic energy of the body at the impact is $\frac{1}{2}V_B^2$:

$$\delta\mathcal{E} = \frac{\Delta\mathcal{E}}{\mathcal{K}} = 2\kappa\left(\frac{V_{\text{sc}}}{V_B}\cos\phi - 1\right) = 2\kappa\varepsilon \tag{11}$$

The maximum energy variation is achieved if $\cos\phi < 0$, i.e. the impact occurs in the anti-velocity direction or with an high relative velocity. Thus, optimization of the KI geometry requires the maximization of $|\varepsilon|$ at the Impact Point, in order to achieve the maximum deflection. Also in this case, a two layer optimization is adopted:

1. In the first layer, again, V_∞ is minimized.
2. In the second layer, instead, taking as initial guess the result of the previous layer, a constrained optimization of ε is performed.

4. Lambert-Based Grid Scan & Mission Scenario Optimization

In this paper a simplified approach based on Lambert Problem is adopted, to address geometries, energies and times involved. This approach is preferred for its simplicity, effectiveness and computational cost, allowing to perform different optimization steps on the whole NEA population group (35000 items, considering real + synthetic

populations). Considering as reference Epoch E_0 the 1st of January 2025, a departure time windows spanning between E_0 and the 31st of December 2040 is considered here. Then, an optimization (based on Lambert problem) is executed to find the $\boldsymbol{\chi} = (E, TOF)$ couple such that a Lambert arc exists and minimizes some objective function $\mathcal{J}$. The objective function is specified depending on the mission scenario. Here E is the delta-Epoch from E_0 and TOF the Time of Flight to the target.

- **RV Mission**: in the case of a rendezvous mission, the objective functions is given by:
$$\mathcal{J}(\boldsymbol{\chi}) = V_\infty^{\text{dep}} + \Delta V_{\text{rv}} \tag{12}$$
- **FB Mission**: the flyby mission scenario is instead characterized by a *two-level* optimization. The *first* level has the objective to find all the V_∞^{dep} minima within the specified launch window, with the following cost function:
$$\mathcal{J}_1(\boldsymbol{\chi}) = V_\infty^{\text{dep}} \tag{13}$$
The *second* level instead is dedicated to the encounter time maximization. This is achieved minimizing the encounter relative velocity $\mathbf{U}$:
$$\mathcal{J}_2(\boldsymbol{\chi}) = ||\mathbf{U}|| \tag{14}$$
In this case a constrained minimization is performed, to limit the V_∞^{dep} within a certain acceptable range. This result in the following NLP problem:
$$\min \mathcal{J}_2(\boldsymbol{\chi}), \quad \text{s.t.} \quad V_\infty^{\text{dep}}(\boldsymbol{\chi}) \in [0, c \cdot V_\infty^{\text{dep}}|_0] \tag{15}$$
where $V_\infty^{\text{dep}}|_0$ is the result of the first optimization level and $a > 0$ a multiplicative factor.
- **KI Mission** in the case of the KI mission, the *two-level* optimization scheme is adopted. The *first* level has the same objective function of the FB case while the *second* level has the objective to maximize the impact effect. This is achieved minimizing
$$\mathcal{J}_2(\boldsymbol{\chi}) = \frac{1}{|\varepsilon|} \tag{16}$$
with the same constrains adopted above.

The *two-level* scheme is preferred for the FB and KI mission scenario due to the fact that NEA may have a relatively high inclination. Then, for this analysis is preferred to look for trajectory with a good *transfer efficiency* rather then of complex, mission specific designs.

To clarify this concept, an example is presented in Fig. 4 where asteroid 2101 Adonis targetting is considered. The *first* level optimization is performed on V_∞^{dep}, which porkchop plot is depicted. Consider, that, for example, the region delimited by the black box in Fig. 4 is the region of interest for a KI mission to Adonis. As a result of the *first* level, 4 points are retrieved (A,B,C,D), sorted in function of their V_∞.

Note that all those points belongs to regions in which $\varepsilon < 0$, while regions in which $\varepsilon > 0$ (green) results in extremely high energy transfers. This is justified by Eq. 11 and by the fact that the most energy efficient impacts would be at $\phi \to \pi$ and not

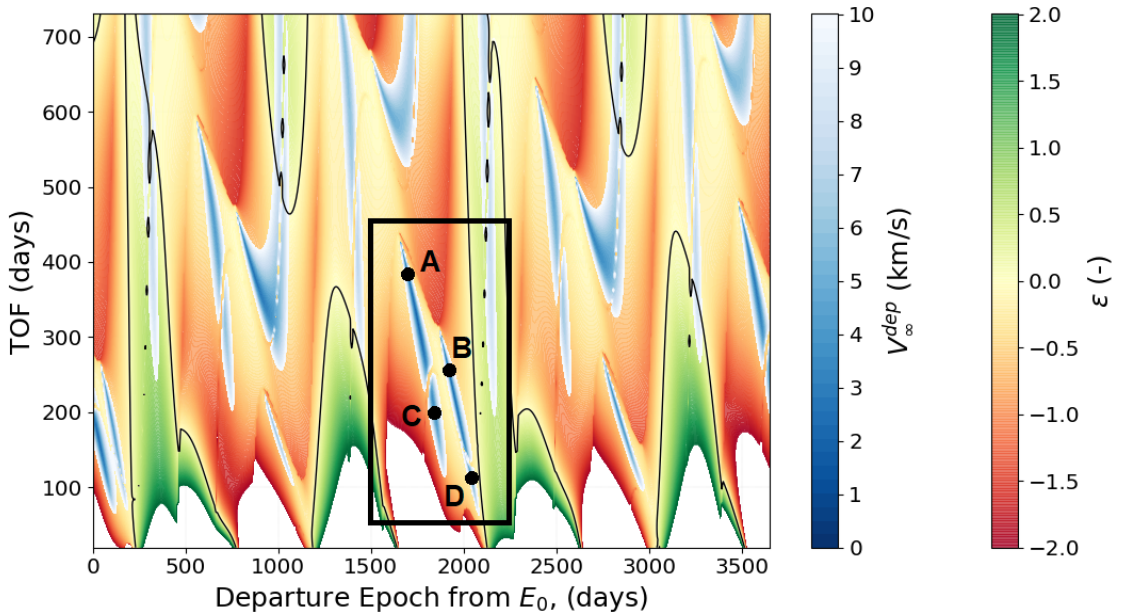

Figure 4. KI scenario *two-level* porkchop plot example: *2101 Adonis* asteroid targetting (a = 1.88 AU, a = 0.76, i = 1.32°). Thin black lines here represent $\varepsilon = 0$, while the black box is the region of interest and the dots local minima.

at $\phi \to 0$. Then the *second* level of the optimization correspond in a constrained maximization of ε in proximity of the points. This would allows the transfer arc to move within the single A, B, C and D regions but not to jump between them, if c of Eq. 15 is properly chosen. As a result of this optimization step, families of (V_∞, ε) couples are retrieved as a function of c. Furthermore, this optimization step can be arbitrarily tuned on the ΔV budget of a specific mission, trying to optimize its objective. Finally, this approach is preferred over a multiobjective optimization for computational reasons (an adaptive mesh algorithm is developed for the first level of optimization initial guess generation resulting is an extremely fast computation of the two levels) as well as over a weighted sum optimization, since *control* on the two layers is desired and no weights dependence is present (less than c, which anyway have a clear physical meaning).

5. Results

In this section the results of the NEA reachability analysis are presented. First, the three mission scenario results are presented and then, the resulting distributions are associated to a simplified direct escape from the Earth-Moon L1 and L2 Libration Points.

5.1. Rendezvous

For the RV case in Fig. 5 the reachable faction of NEAs with a direct transfer is presented. Note that it possible to rendezvous with approximately 60% of the augmented population with a maximum total ΔV of $10\,\mathrm{km/s}$, while the reachable fraction increases to 90% if a maximum ΔV budget of $15\,\mathrm{km/s}$ is considered.

Then, the subset of bodies within a total ΔV of $15\,\mathrm{km/s}$ is extracted ($\sim$90% of the

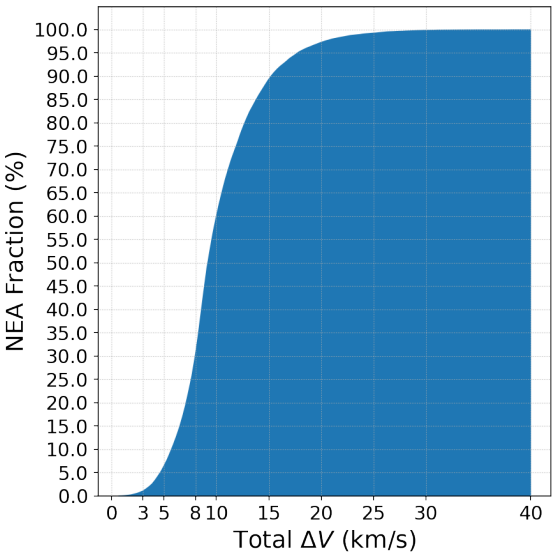

Figure 5. NEA reachable fraction for the rendezvous mission scenario.

population) and their parameters cross correlations analysed by means of a Pearson correlation matrix, represented in Fig. 6a. As a result, note that in this case the to-

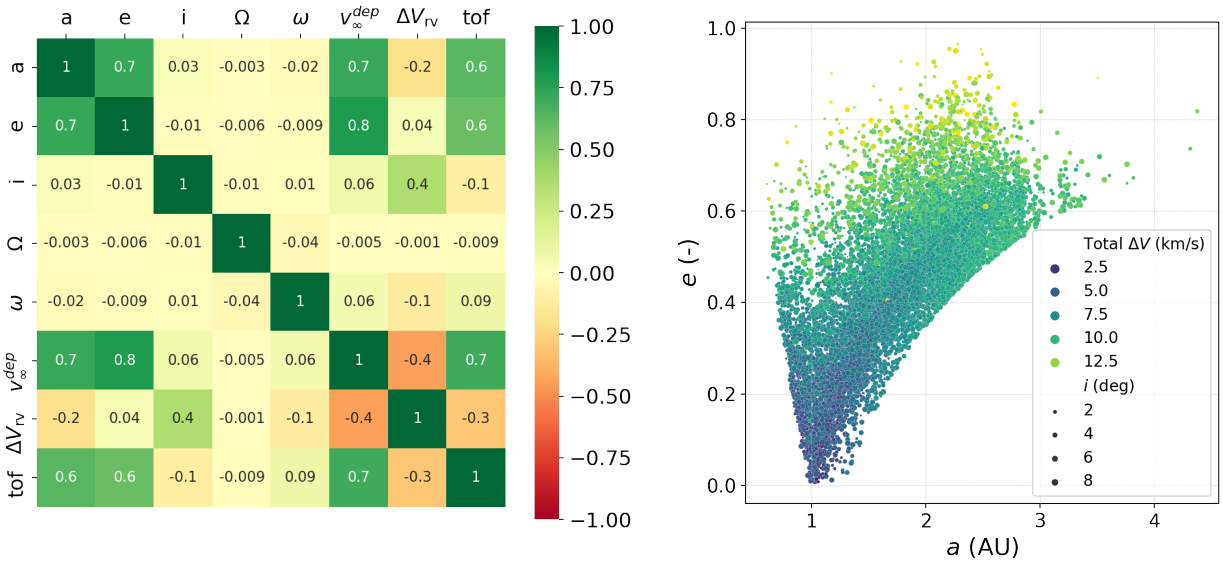

(a) Pearson correlation matrix. **(b) Total ΔV vs (a, e, i).**

Figure 6. Rendezvous results.

tal ΔV is correlated with the target semimajor axis, eccentricity (which influence the departure condition) and inclination (which mostly influence the arrival condition) as well as on the transfer TOF, as can be seen in Fig. 6. Can be shown that as far as the inclination is $<10\,\mathrm{deg}$ it becomes uncorrelated. As final note, Ω and ω seems not to be correlated to any quantities: this is due to the fact that a ”large” launch window is considered. Then if the launch window is tightened, the influence of the initial phase between the bodies may be relevant (and so their RAAN and argument of perigee).

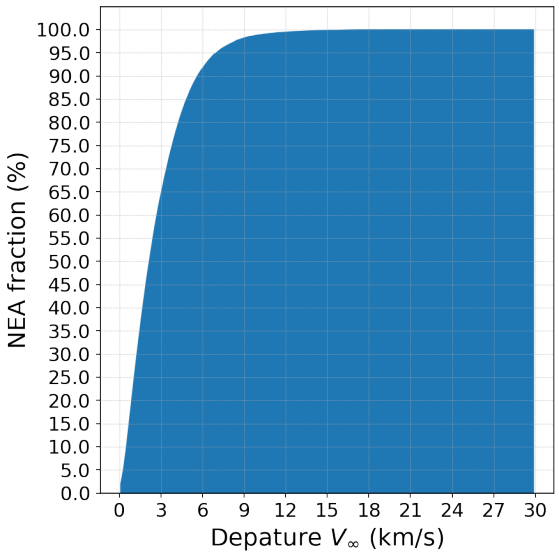

(a) NEA reachable fraction for the flyby mission scenario (c=2).

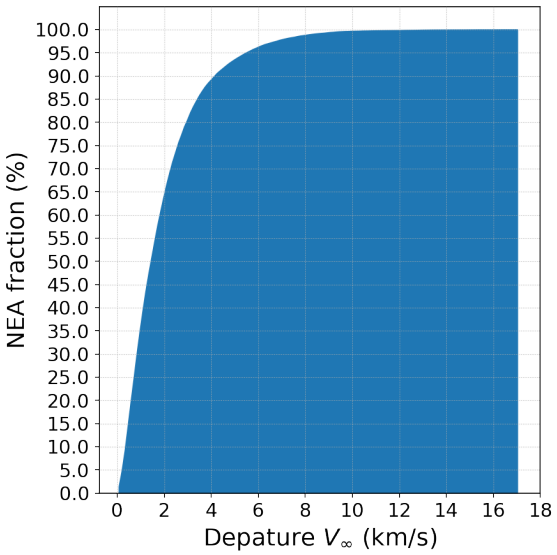

(b) NEA reachable fraction for the kinetic impact mission scenario (c=2).

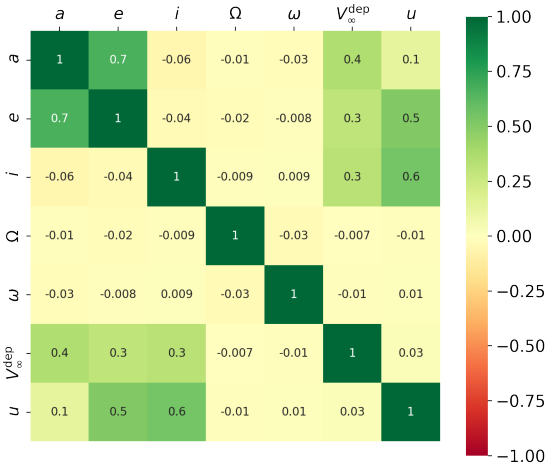

(c) Pearson correlation matrix for the flyby mission scenario (c=2).

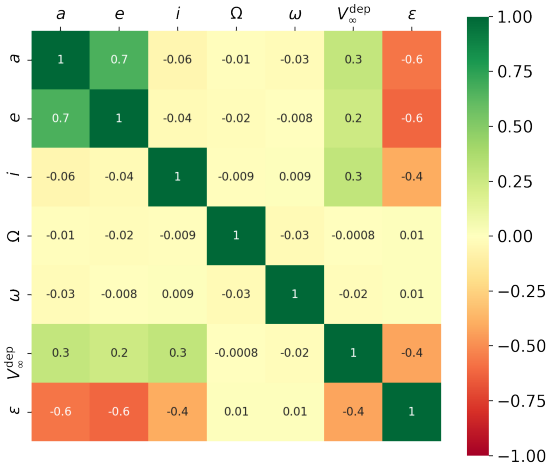

(d) Pearson correlation matrix for the kinetic impact mission scenario (c=2).

Figure 7. Two-levels optimization results.

5.2. Flyby

For the FB case, in Fig. 7a, the reachable fraction of NEAs with a direct transfer is presented. Note that in this case the reachable fraction is much higher, due to the fact that the departure V_∞ is optimized only, so that most encounters happens on the ecliptic plane. Note that this strategy results in the arising of a correlation of V_∞^{dep} and $\mathbf{U}$ to the inclination.

5.3. Kinetic Impact

Finally, for the KI case, in Fig. 7d, the reachable fraction of NEAs with a direct transfer is presented. Note that also in this case the reachable fraction is much higher, due to the fact that the departure V_∞ is optimized only, so that most encounters happens on the ecliptic plane. Note that this strategy results in the arising of a correlation of V_∞^{dep} and $\mathbf{U}$ to the inclination.

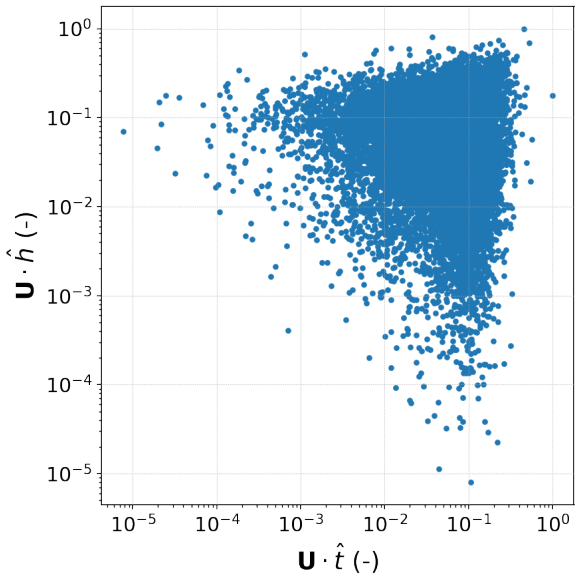

Figure 8. $\mathbf{U}$ along-track and orthogonal normalized components.

In KI and FB cases, in fact, can be seen that the $\Delta\mathbf{V}$ has always a component in the target orbit (local) momentum direction and in some cases this component is dominant over the in-plane component (Fig. 8). In particular, note that if the interest is to increase the only orbital energy, this would correspond to maximize:

$$\Delta\mathcal{E} \approx \kappa V_B \mathbf{U}\cdot\hat{t} \tag{17}$$

which cannot always be achieved with the presented transfer optimization.

5.4. Direct EML1/EML2 Departure Distributions

The computation of the direct escapes from the Earth-Moon L1 and L2 Libration Points is obtained with the following procedure:

1. Assuming to start at one of Earth-Moon Lagrangian Points, a manoeuvre is performed, with a given magnitude ΔV_d and directed with a given angle ϑ, computed positively from the x-axis of the Earth-Moon rotating frame.

2. The trajectory is propagated until it reaches a control surface, defined at a radius $R_{\mathrm{CS}} \sim$ 2Mkm. A maximum escape time of 3 months is considered, to capture also *low-energy*, multi-revolution escape dynamics.

3. The state at the control surface is gathered, to be used as a figure of merit.

A full scan of $360\,\mathrm{deg}$ span for the ϑ angle and a $0.5\,\mathrm{km/s}$ to $2.5\,\mathrm{km/s}$ span for the ΔV_d is performed. Escape trajectories are then extracted as the ones which results to cross the control radius within the prescribed escape window with a osculating eccentricity $e_{\mathrm{EMB}} > 1$. Here $e_{\mathrm{EMB}} = |\mathbf{E}|$ such that:

$$\mathbf{E} = \frac{\mathbf{V} \times \mathbf{H}}{GM_{\mathrm{EMB}}} - \frac{\mathbf{R}}{R} \tag{18}$$

where $\mathbf{R}, \mathbf{V}$ and $\mathbf{H}$ are the inertial position, velocity and momentum of the osculating orbit at the control surface while GM_{EMB} is the gravitational constant of the Earth-Moon system.

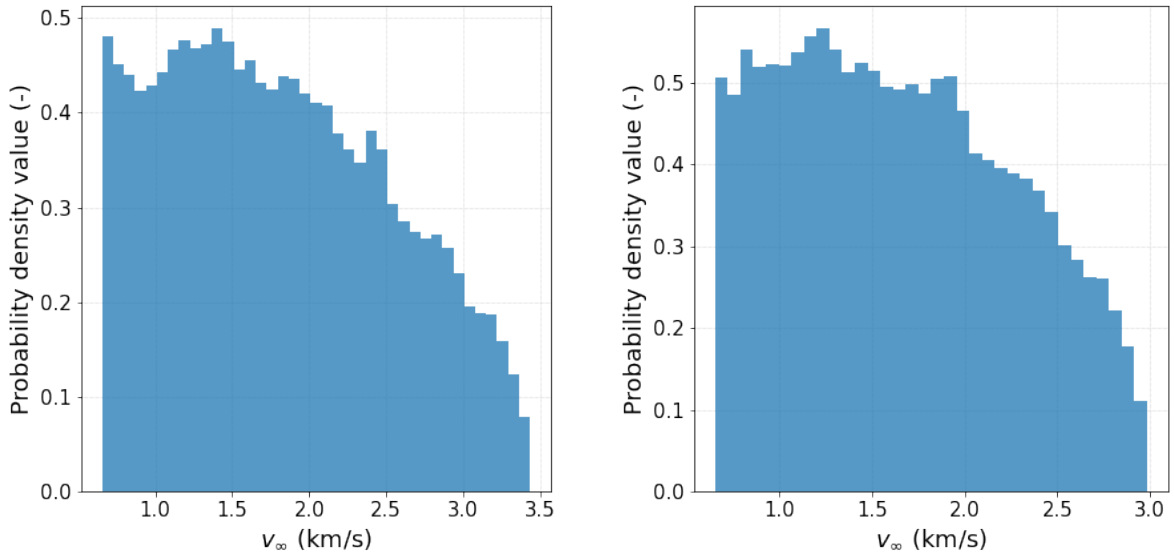

(a) EML2 achievable V_∞s. **(b) EML1 achievable V_∞s.**

Figure 9. Direct EMLP escape hyperbolic excess velocity distributions for $\Delta V_d \in 0.5\,\mathrm{km/s}$ to $2.5\,\mathrm{km/s}$

Note that this approach as the major drawback to not exploiting any kind of Earth or Moon flyby manoeuvre, while due to the Oberth effect, it would be much more efficient to exploit the apses. This can be clearly seen if Fig. 10 where the direct escape *efficiency* for EML1 and EML2 is depicted. Note that most values are < 1, while the only *efficient* escapes are the low-energy ones.

6. Conclusions

In this paper, a reachability analysis of Near-Earth Asteroids from Earth-Moon Lagrangian Points has been presented in three relevant mission scenarios for planetary defence and deep space exploration: rendezvous, flyby and kinetic impact. To summarize, in Table 1 and Table 2 are presented the cumulative reachable fractions of

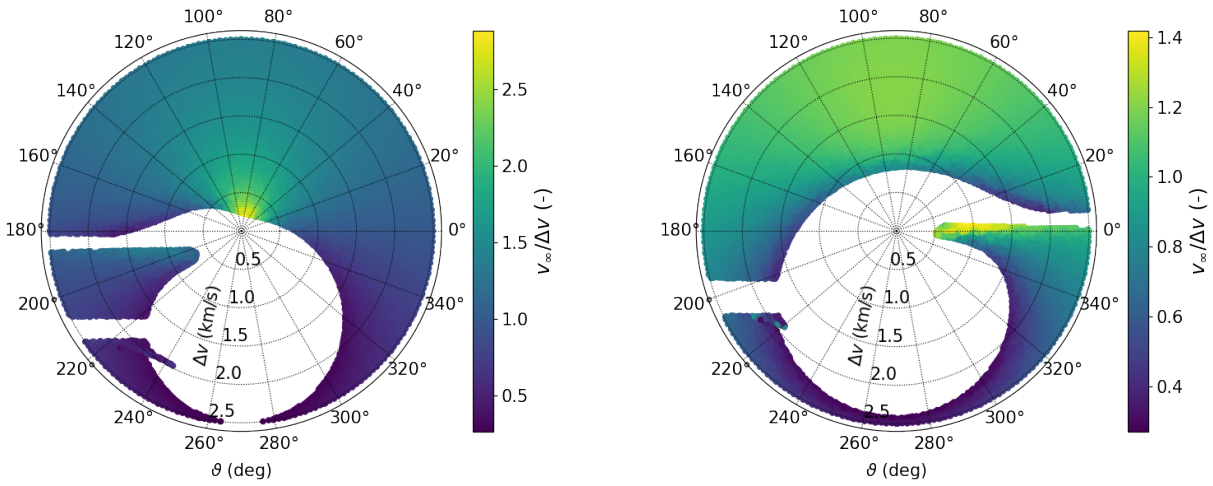

(a) EML2. **(b) EML1.**

Figure 10. Direct EMLP escape *efficiency* for $\Delta V_d \in 0.5\,\mathrm{km/s}$ to $2.5\,\mathrm{km/s}$

Table 1. Augmented population reachable fractions with a ΔV budget of $2.5\,\mathrm{km/s}$

	RV	FB (c=2)	KI (c=2)	KI (c=4)	DEP
EML1	1.09 %	63.32%	80.20%	69.02%	90.28%
EML2	1.86 %	70.28%	85.48%	74.16%	94.52%

objects in case the ΔV available is $2.5\,\mathrm{km/s}$ and $5\,\mathrm{km/s}$ respectively. Here *RV* stays for rendezvous missions, *FB* for flyby mission, *KI* for kinetic impact mission and *DEP* for missions where the only departure energy is optimized. In Table 3, instead the envelope of reachable bodies with low inclination to the ecliptic ($<2\,\mathrm{deg}$) within $2.5\,\mathrm{km/s}$ are presented.

It should be, however, kept in mind that these results refer only to the basic mission profile in which a direct escape from the Earth-Moon Lagrangian Points is achieved, regardless of the phase of the the Earth-Moon system which respect to the Sun-Earth one. Thus the results here presented may be exploited for a fast preliminary assessment of the reachable subset of NEA given a certain ΔV budget, but then the reachability can be enhanced considering more complex escapes (e.g. multi Earth/Moon powered flybys) or specifically-designed heliocentric trajectories (e.g. exploiting Earth-resonant flybys, for example). This, together with the possibility of planning other NEA encounter as a midcourse or *end-of-mission* target may also contribute to increase the number of objects visited even within a low ΔV budget.

References

[1] Grant H Stokes, BW Barbee, William F Bottke, MW Buie, SR Chesley, PW Chodas, JB Evans, RE Gold, T Grav, AW Harris, et al. Update to determine the feasibility of enhancing the search and characterization of neos. *Report of the Near-Earth Object Science Definition Team (Washington, DC: Science Mission Directorate, Planetary Science Division, NASA)*, 2017.

Table 2. Augmented population reachable fractions with a ΔV budget of $5\,\mathrm{km/s}$.

	RV	FB (c=2)	KI (c=2)	KI (c=4)	DEP
EML1	10.04 %	89.50%	95.20%	84.67%	99.38%
EML2	13.58 %	92.15%	96.57%	86.50%	99.76%

Table 3. NEA population reachable fractions, with maximum inclination of $2\,\mathrm{deg}$ (2314 bodies), and a ΔV budget of $2.5\,\mathrm{km/s}$.

	RV	FB (c=2)	KI (c=2)	KI (c=4)	DEP
EML1	6.53%	65.05%	82.00%	70.88%	94.15%
EML2	9.98%	72.82%	87.52%	76.64%	97.22%

[2] Steven R Chesley and Peter Veres. Projected near-earth object discovery performance of the large synoptic survey telescope. *arXiv preprint arXiv:1705.06209*, 2017.

[3] Andrew F Cheng, AG Santo, KJ Heeres, JA Landshof, RW Farquhar, RE Gold, and SC Lee. Near-earth asteroid rendezvous: Mission overview. *Journal of Geophysical Research: Planets*, 102(E10):23695–23708, 1997.

[4] Stefano Campagnola, Naoya Ozaki, Yoshihide Sugimoto, Chit Hong Yam, Hongru Chen, Yosuke Kawabata, Satoshi Ogura, Bruno Sarli, Yasuhiro Kawakatsu, Ryu Funase, et al. Low-thrust trajectory design and operations of procyon, the first deep-space micro-spacecraft. In *25th International Symposium on Space Flight Dynamics*, volume 7, 2015.

[5] DS Lauretta, SS Balram-Knutson, E Beshore, WV Boynton, C Drouet d'Aubigny, DN DellaGiustina, HL Enos, DR Golish, CW Hergenrother, ES Howell, et al. Osiris-rex: sample return from asteroid (101955) bennu. *Space Science Reviews*, 212(1):925–984, 2017.

[6] Sei-ichiro Watanabe, Yuichi Tsuda, Makoto Yoshikawa, Satoshi Tanaka, Takanao Saiki, and Satoru Nakazawa. Hayabusa2 mission overview. *Space Science Reviews*, 208(1):3–16, 2017.

[7] Leslie McNutt, Les Johnson, Pater Kahn, Julie Castillo-Rogez, and Andreas Frick. Near-earth asteroid (nea) scout. In *AIAA Space 2014 Conference and Exposition*, page 4435, 2014.

[8] D.J. Grebow. Generating periodic orbits in the circular restricted three-body problem with applications to lunar south pole coverage, 2006.

[9] Emily M Zimovan, Kathleen C Howell, and Diane C Davis. Near rectilinear halo orbits and their application in cis-lunar space. In *3rd IAA Conference on Dynamics and Control of Space Systems, Moscow, Russia*, volume 20, 2017.

[10] Jacob Williams, David E Lee, Ryan J Whitley, Kevin A Bokelmann, Diane C Davis, and Christopher F Berry. Targeting cislunar near rectilinear halo orbits for human space exploration. 2017.

[11] Shuai Wang, HaiBin Shang, and WeiRen Wu. Interplanetary transfers employing invariant manifolds and gravity assist between periodic orbits. *Science China Technological Sciences*, 56(3):786–794, 2013.

[12] Davide Conte, Marilena Di Carlo, Koki Ho, David B Spencer, and Massimiliano Vasile. Earth-mars transfers through moon distant retrograde orbits. *Acta Astronautica*, 143:372–379, 2018.

[13] Francesco Topputo, Yang Wang, Carmine Giordano, Vittorio Franzese, Hannah Goldberg, Franco Perez-Lissi, and Roger Walker. Envelop of reachable asteroids by m-argo cubesat. *Advances in Space Research*, 2021.

[14] C. Greco, M. Di Carlo, L. Walker, and M. Vasile. Analysis of neos reachability with nano-satellites and low-thrust propulsion. In *Small Satellites, Systems and Services Symposium*, Sorrento, Italy, 2018, 2018.

[15] Joseph Scott Stuart and Richard P Binzel. Bias-corrected population, size distribution, and impact hazard for the near-earth objects. *Icarus*, 170(2):295–311, 2004.

[16] Alan W Harris. On the revision of radiometric albedos and diameters of asteroids. *Icarus*, 126(2):450–454, 1997.

[17] Tarn Duong et al. ks: Kernel density estimation and kernel discriminant analysis for multivariate data in r. *Journal of Statistical Software*, 21(7):1–16, 2007.

[18] Holsapple Keith A. and Housen Kevin R. Momentum transfer in asteroid impacts. i. theory and scaling. *Icarus*, 221, 2012.

[19] AF Cheng, P Michel, Martin Jutzi, AS Rivkin, A Stickle, O Barnouin, C Ernst, J Atchison, P Pravec, DC Richardson, et al. Asteroid impact & deflection assessment mission: kinetic impactor. *Planetary and space science*, 121:27–35, 2016.

[20] KR Housen and KA Holsapple. Momentum transfer in hypervelocity collisions. *LPI*, (1608):2363, 2011.